FILTER BASED ANALYSIS FOR THE MRI DATA IN BIOMEDICAL ENGINEERING

Basavarj Hiremath[1], Lavanya Vaishnavi D A[2], Harish S[3], Anil Kumar C[4]

[1]Assistant Professor Dept of Medical Electronics Engg. Ramaiah Institute of Technology, Bangalore, India, bvhiremath@msrit.edu
[2]Assistant Professor, Dept of ECE R L Jalappa Institute of Technology, Doddaballapur, India. lavanyavaishnavi@gmail.com
[3]Associate Professor, Dept of ECE, R L Jalappa Institute of Technology, Doddaballapur, India. harishsrinivasaiah@gmail.com
[4]Associate Professor & HoD Dept of ECE, R L Jalappa Institute of Technology, Doddaballapur, India. canilkumarc22@gmail.com

Abstract
In biomedical engineering, the enhancement of MRI data is pivotal for precise diagnosis and effective treatment planning. This study presents a filter-based analysis of MRI data, focusing on the application and efficacy of Homomorphic filtering and Gamma filtering techniques. Homomorphic filtering is employed to address the challenges of contrast enhancement and noise reduction by transforming the image into the logarithmic domain, thereby separating the illumination and reflectance components. This approach significantly improves image clarity and consistency, making it easier to identify and analyze anatomical structures. Gamma filtering, on the other hand, adjusts the luminance of MRI images to enhance contrast and visibility of specific features. By optimizing gamma values, we tailored the image quality to highlight different tissue types and pathological conditions. Our comparative analysis reveals that both Homomorphic filters and Gamma filtering offer substantial improvements in the quality of MRI data, each with distinct advantages. Homomorphic filtering excels in noise reduction and standardizing lighting conditions, while Gamma filtering provides flexible contrast enhancement tailored to diagnostic needs. The findings underscore the potential of these techniques to advance the accuracy and reliability of MRI-based diagnostics in biomedical engineering, suggesting further research into their combined application and optimization for automated imaging systems.
Keywords: Biomedical image processing, Filters, MRI data.

1. Introduction

Medical imaging is a process of manipulating the images of interior body parts for the clinical analysis or for the medical intervention. This helps to analyse some of the organs or eternal tissues of the human body. Review medical imaging techniques The details we need to skins and bones are also important for the diagnostics. To identify the abnormalities the medical imaging has an established database for the normal anatomy and physiology. Pathology includes imaging for removed organs or tissue, even in pathology there is a part of manipulating of images or processing of image to extract certain data. There were five billion medical image studying has been carried out worldwide in 2010. It was estimated that the radiation exposure from the medical imaging was up to 50% in 2006 [1], this statistic was taken alone in United States. Many image sensors, biosensors, microcontroller, microprocessor, digital signal processing, and media processes are used to manufacture and medical equipment. The technologies like semiconductors CMOS integration and power semiconductor devices are normally adopted. Nowadays, advanced medical image processing chips are manufactured for the particular purpose. The imaging technique improves the non invasive treatment for the patients [2].

A. Different types of medical imaging

The radiology or the clinical imaging is normally referred with the invisible light medical imaging. In certain visible light medical imaging, it involves the examination of still picture or examination of digital video when it is seen without a special equipment. The two main branches of medical imaging that uses the visible light imagery are the wound care and the dermatology [3].

Based on the context and different research and development areas, the scientific investigation, or the medical imaging, normally divided into different disciplines, like medical physics, medicine and biomedical engineering. The research and development in several areas of instrumentation [4]. And in the process of image acquisition modelling and also the quantification are usually the preserve of biomedical engineering, Computer science and medical physics and also electronics. Radiology is one of the branch of which is used to interpret the medical images. There are several other sub disciplines that are relevant to the conditions of medical sciences that normally perform the investigation on images. There are different techniques that are developed for medical imaging. And they have several scientific and industrial applications as well [5].

B. MRI

Magnetic Resonance Imaging, which is abbreviated as MRI. This is an medical imaging technique that is used in the radiology. The anatomical sections are taken in the form of images. Restaurant magnetic fields are used by the MRI scanner, The magnetic field gradient and the radio we use help us to generate the image of different organs of the body. The main difference between computed tomography and MRI is that it is not involving the X ray for the purpose of ionisation. MRI also have different applications, like nmr spectroscopy apart from the medical imaging [6].

MRI is used in the hospitals for medical diagnostics that helps in staging and also following up for the disease. MRI gives a better contrast when compared with city images on the soft tissues. MRI gives a very clear image when compared to other technologies in the regions of abdomen and brain [7]. However, it is considered to be much less comfortable to the patients due to the louder measurement noise and confining tube. Apart from this, many metal implants and non-removable metals in the body will make a risk [8].

At the beginning, MRI was initially coined as nuclear magnetic resonance imaging, and for the day's nuclear was dropped as it associated with the negative comments. The radio frequency was absorbed by certain atomic nuclei which was placed in the external magnetic field. Resultant is spinning polarisation that is used to reduce the radio frequency coil. In other terms, the magnetic spin of protons in the hydrogen nuclei is the reason for the resonation in radio frequency incident waves. This helps in emitting the coherent radiation with the compact direction, These spinning protons also provide the frequency and phase. The rf antennas can easily recognise the coherent amplified radiation. This which is subjected to the examination. The microscopic polarisation is generated using hydrogen atoms in the research MRI and as well as clinical MRI These MRI can be easily detected using RF antennas. MRI normally locates the fat and the water inside the body [9]. The radio waves are excited using the nuclear spin energy transition, The polarisation in the space is localised using magnetic field gradients. The pulse sequence different contrast are Metres that are used to be generated between the tissues. That is based on relaxation properties of hydrogen atoms within them [10].

There are different versatile techniques in MRI. It was developed in 1970s and 1980s. For biomedical research and diagnostics in medicine [11]. MRI is prominently used. Some of the major applications apart from medical imaging are imaging of non living objects such as mummies and fossils. The Diffusion MRI and the functional MRI are utility of MRI capture neutron track. They capture the blood flow in the respective nervous system [12].

2. Objective

The objective of the complete exercise is to develop an advanced computing tool and the algorithm that can automate the analysis of MRI medical images. The primary objective of this paper is to explore and develop advanced methodologies for the analysis of MRI (Magnetic Resonance Imaging) images, with a focus on their applications in biomedical engineering. The paper aims to achieve the following specific objectives:

Enhance Image Processing Techniques: Develop and optimize algorithms for noise reduction, image segmentation, and contrast enhancement to improve the quality and accuracy of MRI images. Investigate the application of machine learning and deep learning techniques to automate and enhance image processing tasks.

Feature Extraction and Quantitative Analysis: Identify and extract critical features from MRI images relevant to various biomedical applications, such as tissue characterization, tumor detection, and anatomical structure delineation. Develop methods for quantitative analysis of these features to provide precise and objective measurements.

3. Enhance Image Processing Techniques

Develop and optimize algorithms for noise reduction, image segmentation, and contrast enhancement to improve the quality and accuracy of MRI images. Conduct comprehensive validation studies to assess the accuracy, reliability, and clinical relevance of the proposed image analysis techniques [13]. Compare the performance of the developed methods with existing state-of-the-art techniques through experimental studies [14].

While capturing the data from MRI, the tissue thickness varies from slice to slice. The thickness of the tissues will lie between 1millimetre to 10millimetre. The several images taken can be stacked together to make a 3D image, This is a primary job of a physician. Once a 3D image is developed, the radiologist or a physician can rotate the organ in to 360 degree and can be sliced to see the tumour or the lesions within the abdominal region clearly [15]. Many clothes leading to stroke, tumours and haemorrhages can also be captured in this process. This technique can also be used for abnormality detection or the bone fracture or bone tumours and others. By achieving these objectives, the paper aims to contribute to the advancement of MRI-based biomedical engineering, ultimately leading to improved diagnostic accuracy, better patient outcomes, and enhanced understanding of complex medical conditions [16].

4. Literature Survey

The authors in the paper [17], Specify about INSERT, which is called as the world's first clinical SPECT MRI Which is used for brain imaging. The technology behind the construction is scintillation detectors with a silicon photomultiplier readout. The authors demonstrate by using clinical MRI environment for the very first time. The authors are using the standardised version of transmit and receive head coil. They are also using an appropriate selection that is customised for an MRI sequence, This can overcome the mutual interference. the magnetic field inhomogeneity Is introduced using the bulky 50KG tungsten collimator, which is used for the construction of INSERT. There is a MRI specific compatible collimator design, which is in homogeneity and is designed to shimming, leading to many simultaneous acquisitions of the data. The authors are analysing the spec data that is obtained along with the MRI sequence, Once it is evaluated, the spec system performance is also calculated, and the effect on MRI is familiarly recorded.

The paper presents a set of simultaneous spect MRI data, which is obtained using this experiment And it demonstrate the multimodal imaging capability, The state of art technique demonstrate multiple capabilities of MRI imaging, the authors also specify few limitations on the same.

The authors in paper [18], Contribute towards the number of people affecting neurological disorder. Abnormality of the brain is termed as neurological disease or it can be brain dysfunction. The authors mentioned that from past year, the detection of neurological disorder is very difficult task, This task is mostly challenging as the medical technology is not advanced as today. The MRI scan, CT scan and PET scan are different technologies that can be used for the scanning. The regular methods like convolutional neural networks are classified as the best for image feature extraction. The authors in this exercise try to detect the neurological disorder from abnormal brain as well as normal brain set using brain set data of MRI. The convolution neural network algorithm is used to classify the normal brain and the abnormal brain in the MRI data. The state of art technique helps the authors to classify the normal and abnormal brains in an effective way. The efficiency of algorithm is found to be 96.32%.

One of the complicated task in the analysis of brain MRI image is segmentation and analysis of the Tumour structure, This was the main concern for the authors in the paper [19]. This task is considered to be tedious as the tumour are really unpredictable, and the characteristic of tumour region is very much difficult for the computing, as the accurate tumour size, texture and the location cannot be located with simple algorithm. The optimal three phase MRI segmentation framework is one of the novel technique proposed by the authors for the effective interpretation and also for the classification of the MRI data set. The authors also went on for the investigation process of segmented framework under MRI imaging. The Nobel Prize is now intended for the assortment of different services. And it is mostly for the popular FCM cluster framework They authors proposed this framework for the comprehensive tumour analysis. The authors have two levels of details in this exercise. The first level is manifestation and also identification of the tumour within the input data set. The in the 2nd level, the segmentation of the tumour and the analysis is made in the regions of MRI images. The last stage is to construct the tumour region and have an extrapolation which can extract the tumour core. The proposed novel state of our technique is capable of achieving an accuracy of 98. 23% ± 1.1%.

The authors in the paper [20], Clinical magnetic resonance imaging systems have strong magnetic fields of up to 3 Tesla. The human image research system now costs 7 Tesla. This presentation will highlight some of the challenges of measuring the chest, abdomen, and abdomen during these surgeries. One of the best technological advances is the use of various independent methods to perform radio stimulation of tissues.

In paper [21], the incidence of breast cancer has increased every year, and now it is the number one cancer among women, and it is gradually getting younger. MRI-guided interventional diagnosis and treatment of breast cancer has become the focus of research. High field studies show the diagnostic value of breast MRI, but the cost of the test is significantly higher than the cost of conventional mammography. Low-field MRI provides standard MRI contrast with significantly lower costs. For a given pulse frequency and magnetic field strength, the SNR greatly affects the radio frequency coil characteristics. An ideal breast roll should provide good SNR, yet create a uniform B1 area while maintaining patient comfort. RF receiver coil design is the main determinant of image quality, so design and build a low-field breast imaging coil to solve this problem. In this study, a special coil was developed for interventional breast MRI imaging in the 0.35T low-field MRI system, starting from signal reception. The results show that the coil design is suitable for medical intervention procedures and that the coil exhibits better SNR and uniform detection characteristics.

Duchenne muscular dystrophy (DMD) in [22] is a genetic disorder caused by a deficiency of the protein dystrophin. Muscle biopsy is the gold standard for determining disease severity and progression. MRI has shown potential for monitoring disease progression or evaluating the efficacy of treatments. In this study, some quantitative MRI parameters were used to classify tissue components in the canine model of DMD using histoimmunochemical analysis as "ground truth". The results show that several MRI parameters can be used to classify muscle tissue and produce high-resolution tissue type maps that can be used as noninvasive imaging biomarkers for DMD.

The scholars in [23] propose as Prostate cancer is the fourth most commonly diagnosed cancer in the world. TRUS-guided prostate biopsy is painful and inaccurate. Accurate, repeatable, and painless localization of the prostate gland is still needed. Multispectral MRI data from different modalities is currently a promising method for prostate gland localization. However, it is clear that reading these 2D images is difficult. With computerized segmentation, the time required to read 3D images can be reduced, focusing on specific areas and improving biopsy accuracy. For this purpose, three main 3D texture features are used, namely GLCM, LBP and three-dimensional wavelet transform, T1-weighted, T2-weighted and contrast-enhanced data will be used to create a multispectral basis for features. In this paper, all the above-mentioned MRI features are analyzed, and finally, the best 3D features for the classification of prostate tumor regions are examined.

The researchers in [24] have sequential MRI protocols for brain tumor segmentation in clinical practice are not standardized, so flexible segmentation approaches that optimally use available MRI data are needed. In this study, we present and evaluate early and late Convolutional Neural Networks (CNN) based on the DeepMedic architecture using different combinations of multiple MRI sequential databases. For the early fusion approach, we train a special CNN for possible combinations of MRI sequences, while the late fusion approach is a more general approach, in which we train an independent CNN for each type of MRI sequence and fully combine feature maps. layers to create aggregate segmentation. Compared to the early fusion CNN, the segmentation performance of the late fusion approach was very similar, providing more flexibility in terms of combining all available MRI data.

5. Problem Statement

In the field of medical diagnostics, ensuring precise and efficient interpretation of biomedical images—such as MRI, X-rays, and CT scans—is crucial for the early detection, diagnosis, and treatment planning of numerous diseases and injuries. Even though there have been substantial advancements in medical imaging technologies, several persistent challenges hinder the full potential of these diagnostic tools. These challenges include:

High Variability in Image Interpretation: The interpretation of MRI, X-ray, and CT images heavily depends on the expertise of radiologists. Variations in experience and subjective judgment among practitioners can lead to inconsistencies in diagnosis, impacting patient outcomes.

Limited Accessibility to Expert Analysis: In many regions, particularly rural and underserved areas, there is a shortage of skilled radiologists. This limitation hinders timely and accurate diagnosis, delaying the initiation of appropriate treatment plans.

Increasing Volume of Imaging Data: The growing reliance on biomedical imaging for diagnostics has led to a rapid increase in the volume of imaging data. Managing, storing, and analyzing this vast amount of data pose significant logistical and computational challenges.

Detection of Subtle Pathological Features: Early stages of diseases or small lesions can be difficult to detect, and sometimes subtle abnormalities are overlooked. This oversight can lead to delayed treatment with potentially adverse outcomes for patients.

Integration of Multimodal Imaging Data: Different imaging modalities (MRI, X-ray, CT) provide complementary information. However, integrating and correlating data from these diverse sources to improve diagnostic accuracy and patient care remains a complex challenge.

6. Methodology and Results

The figure 2., interprets the generic representation of the proposed algorithm, which includes five different iterations with the point of data collection to comparative analysis by involving the basic steps of the image processing on the three different set of database such as MRI,CT and X-Ray images under consideration, the brief description of the proposed steps are as follows:

A. Gamma Correction:

Gamma correction refers to the controls function responsible for representing the image's overall brightness, which appears to be bleached or too dark [25]. The logic behind the gamma correction technique is to apply a transformation function to the input image so that, contrast factor of the output image is enhanced based on two varying parameters or variables such as c and gamma value γ(Y) between 1.01 to 2.

Thus, gamma can be expressed as a nonlinear relationship between the input - (pixel value) and the resulting output (i.e., brightness or loosely called intensity). The gamma correction transform is given by a functional relationship, which can be expressed as:

$I_{Out} = c\, I^{\gamma}_{In}$ … (eq.1)

The equation (1), c and γ indicate a parameter value used to adjust the transformation function's shape. IOut represents resultant image intensity values (i.e., output image), and IIn represents pre-compensation image data. The parameters c is mostly considered a constant equal to one, and the value of γ varies with different ranges, which generates different stretching effects. The proposed study considers the assignment of gamma value between suitable ranges, i.e., 1.01 to 2. However, the gamma correction sometimes produces an assorted result as it pre-assigned gamma value for each input image. Therefore, the proposed system performs an optimization of gamma correction mechanism to improvise the image's visual quality to acquire enhanced contrast ratio as a pre-processing step. Besides, the optimization approach is implemented by the varying value of gamma from the range between 0.9 to 1.2, which is selected based on the statistical characteristics of each input image [26].

Table 1 illustrates the visualization of the input image and visualization of the computed gamma-corrected image. The obtained gamma-corrected image has better visual quality than the input image. The numerical observation is also given in Table 4.1 to assess and analyze the gamma correction mechanism's performance in GCF, CPP, Contrast, and Sharpness.

Table 1: Numerical observation of input image and gamma-corrected image

Input Image		Gamma Corrected image
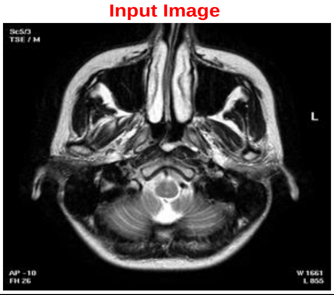		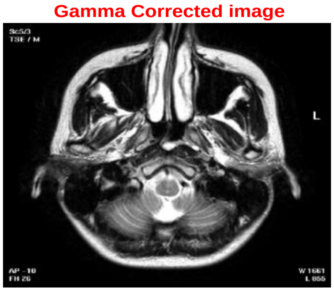
γ- value	--	**1.05**
GCF	**11.7666**	**12.2919**
CPP	**6.2736**	**6.7369**
Contrast	**2.9999**	**3.2568**
Sharpness	**9.0403**	**9.6937**

Table 2 demonstrates the different accuracy values with respect to different gamma values (Step17).

Table 2: Illustration of T (table)

Gamma Value (γ)	v1- (GCF)	v2- (CPP)	v3- (Contrast)	v4- (Sharpness)
0.9	7.19	2.47	1.13	3.39
0.95	8.19	3.14	1.47	4.42
1	9.39	4.00	1.91	5.76
1.05	10.76	5.09	2.48	7.51
1.10	12.22	6.43	3.18	9.51
1.15	13.17	7.70	3.74	10.56
1.2	13.70	8.76	4.12	11.27

B. Computing Procedure for Gamma Correction

i). Loading Input value

*Step-1. Initialize I_m(Input image) →**global***

Step-2. Load Image from database

Step-3. Read→ Image

Step-4. Perform of RGB image to Grayscale Image conversion

a. Check : size of Input image = 3

b. Convert: Input image to gray

Step-5. Display Input image

ii). Applying Gamma Correction

Step-6. Initialize variable I_γ

Step-7. Assign I_γ →double(I_m)

Step-8. Assign Value for γ

a. γ →Select between a range of 0.01to 2

Step-9.Compute I_γ→ $(I_\gamma)^\gamma$

Step-10.Perform Normalization ←I_γ

Step-11.Compute GCF, CPP, Contrast, and Sharpness

*Step-12. Initialize variable v1, v2, v3, v4, T →**Global***

Step-13. Create empty matrix [] ← v1, v2, v3, v4, T

Step-14. For each value of γ between 0.9 to 1.2

Step-15. Repeat the above process ("Step6 to Step11")

Step-16. Assign GCF→ v1, v2 →CPP, v3 →Contrast, v4→ Sharpness

Step-17. Store value of γ with respect to *v1, v2, v3, v4 →T*

Step-18. Perform Reconstruction of v1, v2, v3, v4

Step-19. Select an optimal mechanism

V→ $[v_R1;\ v_R2]^{Transpose}$

S →fs (V, 2)/2

Step-20. Compute the best index(b_i)

bi→ S==fmax(S)

γi →T(bi, 1)

Step-21.IγOpt →(Iγ)γi

Step-22. Perform Normalization ←IγOpt

iii) Optimization of Gamma Corrected Image

Finally, gamma-corrected optimization is achieved using recently computed gamma value (Step-21 and Step-22), shown in Table 3.

Table 3 Numerical observation of the optimized gamma-corrected image

<table>
<tr><td colspan="2">Input Image
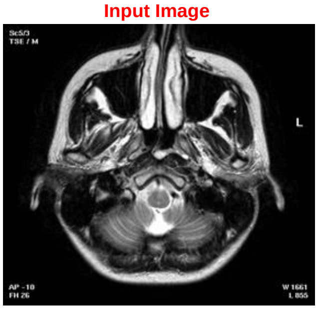</td><td>Gamma Corrected image
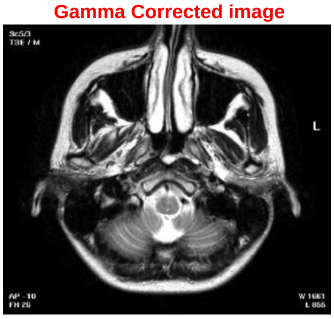</td><td>Optimized Gamma Corrected Image
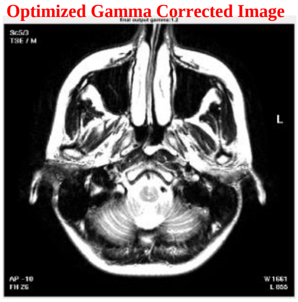</td></tr>
<tr><td>γ- value</td><td>---</td><td>1.05 (user selection)</td><td>1.2 (optimal)</td></tr>
<tr><td>GCF</td><td>11.7666</td><td>12.2919</td><td>13.7087</td></tr>
<tr><td>CPP</td><td>6.2736</td><td>6.7369</td><td>8.7660</td></tr>
<tr><td>Contrast</td><td>2.9999</td><td>3.2568</td><td>4.1227</td></tr>
<tr><td>Sharpness</td><td>9.0403</td><td>9.6937</td><td>11.2728</td></tr>
</table>

C. Homomorphic Filtering

Homomorphic filtering is a method for recovering a degraded image having uneven illumination due to a multiplicative random signal. The concept of homomorphic filtering in the proposed framework utilizes an illumination-reflection model in the image enhancement process. This model considers that an image is an array of measured light intensities and is a function of the total light reflected by an object in the scene.

D. Computing Procedure for Homomorphic filtering

This section illustrates computing steps for applying Homomorphic filtering operation on the input image followed by three sequential steps such as Constructing filter, Applying Constructed Homomorphic filter on the input image, and Homomorphic optimization filter.

i). Constructing Homomorphic filter

Step-22. Load $\rightarrow I_m$
a. Go to Step1 to Step5
Step-23. Initialize variable α_{Lf}, α_{Hf} *(low and high-frequency gain),* f_{odr}*(filter order)*
Step-24. Assign a value for f_{odr}
a. $f_{odr} \rightarrow$ *Select from the range of 0.5 to 5*
Step-25. Compute the size of the image
a. I_m *(Size)* $\rightarrow [\,]_{row\times colm}$
Step-26. Compute Homomorphic filter (Hm_f*)*
a. Create an array A of zeros as per the dimension of the image
b. Compute A
c. Construct Homomorphic filter(Hm_f*)*

ii). Applying Constructed Homomorphic filter on the input image

Step-27. Apply Homomorphic filter-(Hm_f*) on* I_m
Step-28. Assign a value of α_{Hf}, α_{Lf}
a. α_{Hf}, α_{Lf} $\rightarrow$ *Select between a range of 0.05 to 2*
Step-29. Compute Homomorphic filtered image-(Hm_f*-*I_m*)*
a. $Hm_f \rightarrow ((\alpha_{Hf} - \alpha_{Lf}) \times Hm_f) + \alpha_{Lf})$
b. $Hm_f \rightarrow Hm_f - 1$
Step-30. Calculate log of I_m*-(*I_{mLOG}*)*
Step-31. Calculate DFT of I_{mLOG}
Step-32. Assign filtering on DFT I_m
Step-33. Perform inverse of DFT on filtered I_m
Step-34. Perform inverse log
Step-35. Perform Step-10 and Step-11
Step-36. Display Hm_f*-*I_m

iii) Optimization of Homomorphic filtered image

Step-37. Initialize variable as in Step-12
Step-38 Create an empty matrix as in Step-13
Step-39 Initialize kx to store all possible values of f_{odr}
Step-40. for α_{Hf}, α_{Lf}, f_{odr}
Step-41. Assign value with a specified range
a. $\alpha_{Lf} \rightarrow 0.8$ *to 1.1*
b. $\alpha_{Hf} \rightarrow 0.8$ *to 1.1*
c. $f_{odr} \rightarrow 0.5$ *to 6*
Step-42. Compute H_{mf}*-* I_m *using* α_{Hf}, α_{Lf}, f_{odr} *and* I_m
Step-43. Compute Accuracy outcome
a. GCF, CPP, Contrast, Sharpness
Step-44. Assign a value of computed Accuracy outcome into Empty Matrix (Step-38)
a. v1 $\leftarrow$ *GCF*
b. v2 $\leftarrow$ *CPP*
c. v3 $\leftarrow$ *Contrast*
d. v4 $\leftarrow$ *Sharpness*
Step-45. Assign value Computed α_{Hf}, α_{Lf}, f_{odr} *with respect to v1, v2, v3, v4* $\rightarrow T$
Step-46. Perform Reconstruction of v1, v2, v3, v4
Step-47. Select an optimal mechanism
a. $V \rightarrow [v_{R1};\ v_{R2};\ v_{R3};\ v_{R4}]^{Transpose}$
b. $S \rightarrow fs\,(V, 2)/4$
Step-48. Compute fine indexing(f_i*)*
a. $F_i \rightarrow fmax(\,S)$
b. $f_{odr} \rightarrow T(f_i, 1)$
c. $\alpha_{Lf} \rightarrow T(f_i, 1)$
d. $\alpha_{Hf} \rightarrow T(f_i, 1)$
Step-49. Compute H_{mf}*-*I_m $\rightarrow$ *Repeat process as shown in Step-29 to Step-34*
Step-50. Perform Normalization $\leftarrow H_{mf}$*-*I_m
Step-51. Compute Accuracy $\rightarrow$ *GCF, CPP, Contrast, Sharpness*

The Table 4 exhibits the visualization of input image and visualization of computed Homomorphic filtered image using parameter $\alpha_{Lf} = 0.15$, $\alpha_{Hf}=1.39$, and $f_{odr}=2$. It can be seen that the filtered image has better brightness in terms of the increased reflectance effect than the luminance effect. The numerical observation is also given in Table 4.4 to assess and analyze the gamma correction mechanism's performance in GCF, CPP, contrast, and sharpness.

Table 4 Numerical observation of input image and Homomorphic filtering image

Input Image

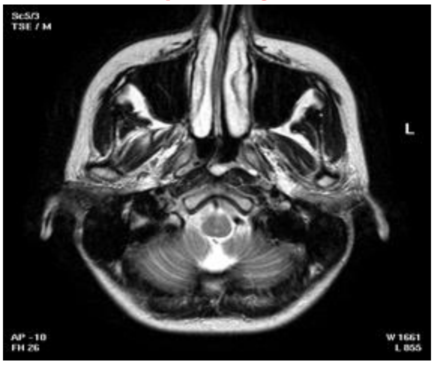

Homomorphic Filtered Image

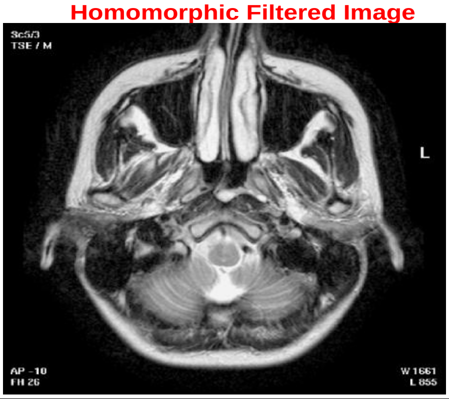

Accuracy	Value	α_{Lf}=0.15	α_{Hf}=1.39	f_{odr}=2
GCF	**11.7666**	**11.5513**		
CPP	**6.2736**	**8.3691**		
Contrast	**2.9999**	**3.3049**		
Sharpness	**9.0403**	**9.6221**		

Table 4 demonstrates the table's structure as a sample because it is quite impractical to demonstrate such a large dimension (432 x 5) of the table, which contains different accuracy values with respect to different parameter values (Step-45).
Table 5 demonstrates a sample of all possible values computed for f_{odr} within the range 0.5 to 5 α_{Hf}, and α_{Lf} within range of 0.8 to 1.1. However, table T has shown only a few randomly selected values from a computed T set because it is challenging to demonstrate here due to its large size, as we already mentioned above. After computing all possible values with different accuracy scores, the proposed system initiates the optimization process. Therefore, the next step towards the optimization process is the reconstruction using function f_{max} over (v1, v2, v3, v4) (Step-46). After obtaining the reconstructed v1, v2, v3, and v4, the next process executes to perform a selection of optimal mechanism which is constructed using the transpose of v1, v2, v3, and v4 (equation (4.8)) to represent them in a column vector for computing sum part of V. The sum part of V is carried out using function f_s over V which refers to carry a summation of considering specified dimension, i.e., 2 (Step-47). The next important step is executed to compute fine indexing for selecting the optimal value of each parameter for homographic filtering, as shown in computing Step-48. Finally, optimization on the homographic filter image is achieved using the recently computed best indexing parameter and executing prior strategy, i.e., Step-29 to Step-36.

Table 5 Sample Illustration of Table-(T)

f_{odr}	α_{Lf}	$\alpha_{Hf,}$	v1- (GCF)	v2- (CPP)	v3- (Contrast)	v4- (Sharpness)
0.5	0.08	0.08	11.54	5.0903	2.73	8.416
1	0.08	0.28	11.64	6.00	2.911	8.80
1.5	0.28	0.08	11.48	5.04	2.70	8.33
2	0.28	0.28	11.75	6.11	2.96	8.96
2.5	0.28	0.08	11.50	5.06	2.71	8.37
3	0.48	0.08	11.48	5.03	2.70	8.33
3.5	0.68	0.28	11.70	6.05	2.93	8.88
4	0.88	0.28	11.67	6.02	2.92	8.84
4.5	0.4	1.08	11.56	12.27	3.93	11.02
5	0.88	1.08	11.71	12.4	4.01	11.24

Optimization of Homomorphic filtered image: This process refers to performing an optimization process to achieve optimal $f$odr value and another parameter to be applied to the input image to obtain an optimal resolution with bright visibility features. The above presented computational step initializes the v1, v2, v3, v4, and T(table), which is further assigned with the empty matrix having one dimension equivalent to zero and it has no row and column (Step-37 and Step-38). The construction of an empty matrix for the initialized variable can be represented using the equation (4.24)

$v1 = [\ ]_{0x0}$; $v2 = [\ ]_{0x0}$; $v3 = [\ ]_{0x0}$; $v4 = [\ ]_{0x0}$ and $T = [\ ]_{0x0}$ ... eq:2

Table 6 identified that the optimized image had increased brightness considering optimal value for each parameter, i.e.,

αLf =0.08, αHf=1.08 and $f$odr=5. Moreover, it can also be analyzed that there is no significant difference between the GCF parameter of non-optimized filtered images and optimized filter images. However, other accuracy parameters such as CPP, contrast, and sharpness have gained higher scores than the accuracy score of both input and non-optimized Homomorphic filtered images.

Table 6 Numerical observation of input image and Homomorphic filtering image

Input Image 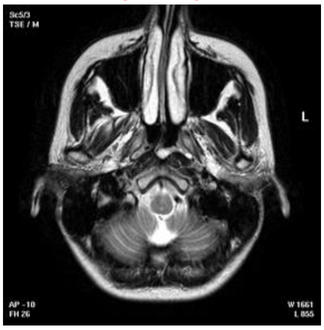		Homomorphic Filtered Image 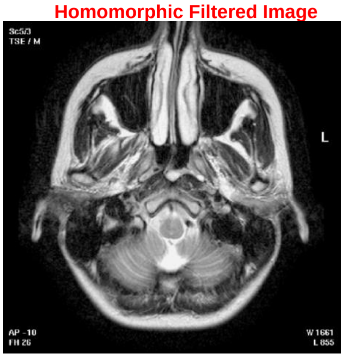			Optimized Homomorphic Filtered Image 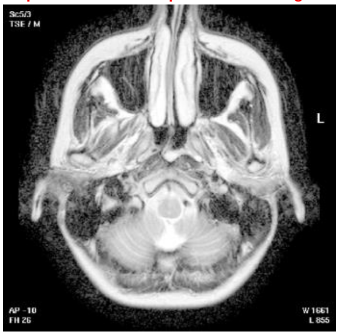		
Accuracy	**Value**	**α_{Lf}=0.15**	**α_{Hf}=1.39**	**f_{odr}=2**	**α_{Lf}=0.08**	**α_{Hf}=1.08**	**f_{odr}=5**
Input Image		**User Selection**			**Optimal**		
GCF	**11.7666**	**11.5513**			**11.7271**		
CPP	**6.2736**	**8.3691**			**12.5915**		
Contrast	**2.9999**	**3.3049**			**4.0464**		
Sharpness	**9.0403**	**9.6221**			**11.3461**		

7. Conclusion

This study underscores the significant potential of Homomorphic filtering and Gamma filtering in enhancing MRI data for biomedical engineering applications. Our analysis revealed that both techniques offer substantial improvements in image quality, each with unique strengths that contribute to more accurate and reliable diagnostics. Homomorphic filtering excels in addressing the challenges of contrast enhancement and noise reduction. By transforming MRI images into the logarithmic domain and separating illumination from reflectance, this method enhances image clarity and consistency. This standardization of lighting conditions across the image improves the visibility of anatomical structures, facilitating better diagnostic interpretation and analysis.

Gamma filtering, conversely, provides a flexible approach to contrast enhancement by adjusting the luminance of MRI images. This method allows for the fine-tuning of image contrast to highlight specific tissue types and pathological conditions. The ability to optimize gamma values for different diagnostic needs makes Gamma filtering a versatile tool in the imaging arsenal of biomedical engineers. Our findings indicate that combining these two techniques could offer a comprehensive solution to the challenges of MRI image enhancement. While Homomorphic filtering addresses global image inconsistencies and noise, Gamma filtering can be applied to further refine contrast and highlight critical features. This dual approach could maximize the diagnostic utility of MRI images, leading to more accurate and effective medical evaluations.

Future research should focus on integrating Homomorphic and Gamma filtering into automated imaging systems, optimizing their parameters for various medical applications. This integration has the potential to significantly advance the field of biomedical imaging, improving diagnostic accuracy and patient outcomes.

References

1. *J. Morahan et al., "Challenges in Acquiring Clinical Simultaneous SPECT-MRI on a PET-MRI Scanner," in IEEE Transactions on Radiation and Plasma Medical Sciences, vol. 7, no. 7, pp. 755-763, Sept. 2023, doi: 10.1109/TRPMS.2023.3287639.*
2. *V. Tyagi and A. K. Ahlawat, "To Detect Normal and Abnormal Neurological Disorder of MRI Image in Human using Convolutional Neural Netwok," 2019 International Conference on Issues and Challenges in Intelligent Computing Techniques (ICICT), Ghaziabad, India, 2019, pp. 1-4, doi: 10.1109/ICICT46931.2019.8977683.*
3. *V. Tyagi and A. K. Ahlawat, "To Detect Normal and Abnormal Neurological Disorder of MRI Image in Human using Convolutional Neural Netwok," 2019 International Conference on Issues and Challenges in Intelligent Computing Techniques (ICICT), Ghaziabad, India, 2019, pp. 1-4, doi: 10.1109/ICICT46931.2019.8977683.*
4. *K. Bhima, M. Neelakantappa, K. D. Ramaiah and A. Jagan, "An OTP Framework for effective tumor segmentation*

and analysis in brain MRI images," 2023 Third International Conference on Advances in Electrical, Computing, Communication and Sustainable Technologies (ICAECT), Bhilai, India, 2023, pp. 1-7, doi: 10.1109/ICAECT57570.2023.10118149.

5. *K. Bhima, M. Neelakantappa, K. D. Ramaiah and A. Jagan, "An OTP Framework for effective tumor segmentation and analysis in brain MRI images," 2023 Third International Conference on Advances in Electrical, Computing, Communication and Sustainable Technologies (ICAECT), Bhilai, India, 2023, pp. 1-7, doi: 10.1109/ICAECT57570.2023.10118149.*
6. *M. E. Ladd et al., "In vivo MRI of the human torso at 7 Tesla using multi-channel transmit," 2010 IEEE International Symposium on Biomedical Imaging: From Nano to Macro, Rotterdam, Netherlands, 2010, pp. 572-572, doi: 10.1109/ISBI.2010.5490283.*
7. *Q. Liu, D. Huiyu, Z. Qing, Z. Yufu, Y. Lier and Y. Kecheng, "Design and Study of the Customized Breast Receiving Coil for Interventional MRI at 0.35T," 2021 IEEE International Conference on Medical Imaging Physics and Engineering (ICMIPE), Hefei, China, 2021, pp. 1-6, doi: 10.1109/ICMIPE53131.2021.9698907.*
8. *Eresen, S. McConnell, S. M. Birch, J. F. Griffin, J. N. Kornegay and J. X. Ji, "Tissue classification in a canine model of Duchenne Muscular Dystrophy using quantitative MRI parameters," 2017 39th Annual International Conference of the IEEE Engineering in Medicine and Biology Society (EMBC), Jeju, Korea (South), 2017, pp. 4066-4069, doi: 10.1109/EMBC.2017.8037749.*
9. *K. Chaisaowong and M. Kitza, "3D-Texture-Segmentation of Prostate Cancer from Multimodal MRI Data," 2021 18th International Conference on Electrical Engineering/Electronics, Computer, Telecommunications and Information Technology (ECTI-CON), Chiang Mai, Thailand, 2021, pp. 525-528, doi: 10.1109/ECTI-CON51831.2021.9454692.*
10. *M. Rahimpour, K. Goffin and M. Koole, "Convolutional Neural Networks for Brain Tumor Segmentation Using Different Sets of MRI Sequences," 2019 IEEE Nuclear Science Symposium and Medical Imaging Conference (NSS/MIC), Manchester, UK, 2019, pp. 1-3, doi: 10.1109/NSS/MIC42101.2019.9059769.*
11. *P. Brocken, B. A. Kiers, M. G. Looijen-Salamon et al., "Timeliness of lung cancer diagnosis and treatment in a rapid outpatient diagnostic program with combined 18FDG-PET and contrast enhanced CT scanning," Lung Cancer, vol. 75, no. 3, pp. 336–341, 2012.*
12. *P. Vivekanandan, "An efficient SVM based tumor classification with symmetry non-negative matrix factorization using gene expression data," in In 2013 International conference on information communication and embedded systems (Icices), pp. 761–768, IEEE, USA, February 2013.*
13. *J. D'Cruz, A. Jadhav, A. Dighe, V. Chavan, and J. Chaudhari, "Detection of lung cancer using backpropagation neural networks and genetic algorithm," Computing Technologies and Applications, vol. 6, pp. 823–827, 2016.*
14. *J. Shen, J. Wu, M. Xu, D. Gan, B. An, and F. Liu, "A hybrid method to predict postoperative survival of lung cancer using improved SMOTE and adaptive SVM," Computational and Mathematical Methods in Medicine, vol. 2021, Article ID 2213194, 15 pages, 2021.*
15. *S. Mandal and I. Banerjee, "Cancer classification using neural network," International Journal, vol. 172, pp. 18–49, 2015.*
16. *D. M. Abdullah, A. M. Abdulazeez, and A. B. Sallow, "Lung cancer prediction and classification based on correlation selection method using machine learning techniques," Qubahan Academic Journal, vol. 1, no. 2, pp. 141–149, 2021.*
17. *F. Taher, N. Prakash, A. Shaffie, A. Soliman, and A. El-Baz, "An overview of lung cancer classification algorithms and their performances," IAENG International Journal of Computer Science, vol. 48, no. 4, 2021.*
18. *Jaweed and F. Siddiqui, "Implementation of machine learning in lung cancer prediction and prognosis: a review," in Cyber Intelligence and Information Retrieval, pp. 225–231, India, 2022.*
19. *V. N. Jenipher and S. Radhika, "SVM kernel methods with data normalization for lung cancer survivability prediction application," in In 2021 Third International Conference on Intelligent Communication Technologies and Virtual Mobile Networks (ICICV), pp. 1294–1299, IEEE, Canada, February 2021.*
20. *V. A. Binson, M. Subramoniam, Y. Sunny, and L. Mathew, "Prediction of pulmonary diseases with electronic nose using SVM and XGBoost," IEEE Sensors Journal, vol. 21, no. 18, pp. 20886–20895, 2021.*
21. *R. Manju, V. Athira, and A. Rajendran, "Efficient multi-level lung cancer prediction model using support vector machine classifier," in In IOP Conference Series: Materials Science and Engineering, vol. 1012, India, 2021no. 1, Article ID 012034IOP Publishing.*
22. *P. Nanglia, S. Kumar, A. N. Mahajan, P. Singh, and D. Rathee, "A hybrid algorithm for lung cancer classification using SVM and neural networks," ICT Express, vol. 7, no. 3, pp. 335–341, 2021.*
23. *S. Harish, C. Anil Kumar, Lakshmi Shrinivasan, S. Rohith, Belete Tessema Asfaw, "Algorithm for Recognition of Movement of Objects in a Video Surveillance System Using a Neural Network", Journal of Engineering, vol. 2022, Article ID 8216221, 4 pages, 2022. https://doi.org/10.1155/2022/8216221*
24. *Harish. S., R. Verma, G. K. Venkatesh, L. Vaishnavi D. A., and A. Kumar C., "Intelligent Filtering Techniques for Reducing Various Noise in Image of Mango Leaves.", Int J Intell Syst Appl Eng, vol. 12, no. 4s, pp. 367–374, Nov. 2023.*
25. *M. Yakar, D. Etiz, M. Metintas, G. Ak, and O. Celik, "Prediction of radiation pneumonitis with machine learning in stage III lung cancer: a pilot study," Technology in Cancer Research & Treatment, vol. 20, p. 153303382110163, 2021.*
26. *N. Maleki, Y. Zeinali, and S. T. A. Niaki, "A k-NN method for lung cancer prognosis with the use of a genetic algorithm for feature selection," Expert Systems with Applications, vol. 164, article 113981, 2021.*